Proceedings of the ASME 2026
45th International Conference on Ocean, Offshore and Arctic Engineering
OMAE2026
June 7–12, 2026, Tokyo, Japan

OMAE2026-XXXX

WIND FARM DESIGN UNDER UNCERTAINTY: MANAGING UNKNOWN NEIGHBORING FARM EFFECTS

Julian Quick[1,*], Pierre-Elouan Réthoré[1], Liza Maak[1], Priyank Maheshwari[2]

[1]Technical University of Denmark, Roskilde, Denmark
[2]TotalEnergies, Paris, France

ABSTRACT

Wind farm wakes can persist for tens of kilometers, reducing downstream farm performance. This "wind theft" is an increasing concern, yet there is little guidance on addressing it during development. We present a framework for wind farm design under uncertainty in neighboring farm characteristics. Using the Danish energy island cluster as a case study, we perform sensitivity analysis to quantify the importance of neighbors' construction timing, turbine type, and layout on project revenue. Construction timing emerges as the dominant uncertainty driver. Analysis reveals that overly pessimistic assumptions about neighbor arrival may substantially undervalue projects. We optimize layouts under conservative (all neighbors present) and liberal (no neighbors) bounding scenarios using the TOPFARM stochastic gradient descent optimization algorithm. No significant design trade-offs are found, indicating that optimal layouts are robust to neighboring farm uncertainty. This simplifies practical design decisions: developers can optimize without precise knowledge of competitor timelines.

Keywords: Offshore Wind Farm Design, Uncertainty, Neighboring Wind Farms

1. INTRODUCTION

Wind energy is becoming an increasingly large part of the world's energy supply. It is expected to account for 35% of US electricity demand by 2050 [1]. There are ambitious plans to build a large set of offshore wind farms in the North Sea, where farm-to-farm interactions are expected to strongly influence energy production. Wind farm wakes can last tens of kilometers [2], significantly affecting downstream wind farms. This energy lost due to farm-to-farm effects is challenging to estimate due to the complex physics involved [3]. There is significant uncertainty in engineering wind farm models [4], and there is no widely-accepted wind farm wake model [5]. This issue is compounded by uncertainty in the planning and operations of competitors. For example, the environmental assessment of the Outer Dowsing Offshore Wind farm highlighted the danger of wakes negatively impacting the neighboring Hornsea II wind farm [6].

There is substantial uncertainty in energy yield and revenue resulting from lack of knowledge of neighboring wind farm characteristics. This requires computationally-expensive high-fidelity models to accurately characterize neighboring wind farm effects. Moreover, it is necessary to make assumptions about the neighboring wind farm characteristics for analysis and design of a target wind farm development. The most conservative approach is to assume all possible neighboring wind farms will certainly be present during the operational life of the wind farm. The most liberal assumption is that the target wind farm will operate in isolation, and neighboring wind farm effects have zero impact.

In this study, we propose a computational framework for quantifying uncertainty due to neighboring wind farm characteristics. This includes defining appropriate probability distributions, reporting the sensitivity of wind farm revenue to these distributions, and optimizing the layout of the farm to be robust to uncertainty in neighboring wind farm characteristics. While the specific numerical results are conditional on models that carry substantial uncertainty, the primary contribution is a computational framework that enables rapid scenario testing as modeling practices evolve and site-specific data becomes available.

The remaining of the paper is the following. Section 2 outlines the methods and case study employed in this study. Section 3 discusses the analysis results. The study is concluded in Section 4.

2. METHODOLOGY

Wind farm clusters challenge many of the assumptions of engineering wake models, and it is becoming increasingly common to use high-fidelity models to approximate these large scale effects. In this study, the wake effects of nearby wind farms are approximated using the TurboPark model [7]. This model is not calibrated to reflect farm-to-farm interactions. As an attempt to conservatively capture wake effects, the Turbopark wake expansion parameter has been reduced to 0.02, making turbine wakes

*Corresponding author: juqu@dtu.dk
Documentation for `asmeconf.cls`: Version 1.45, January 15, 2026.

longer lasting and more concentrated. This is done in an effort to make the wake model more conservative.

In this study we differentiate between nominal power, which has no wakes, external losses, where only neighboring wind farm turbine wakes are simulated, internal losses, where the neighboring wind farm wakes are not considered, and total wake losses, which considers all wind turbine wakes. These definitions are summarized in Table 1.

TABLE 1: Definitions of wake loss quantities examined in this study

Quantity	Definition
No Wake Losses	Assumes no turbines create wakes
Internal Losses	Only model target turbines wake effects, ignore neighboring wind farms
External Losses	Model external wind turbines operating normally and internal turbines operating with zero thrust, isolating the effects of neighboring turbines' wakes
Total Wake Losses	Models all neighboring and target wind turbine wakes

The revenue is modeled based on a power-purchase-agreement or contract-for-difference scheme, where a constant price of electricity is assumed. In principle the revenue can be modeled for any assumed payment structure,

$$R(T) = \int_0^T \sum_{i=1}^{N_t} P[u_i(t), \theta(t)] V(t) \frac{dt}{(1+\delta)^t} \tag{1}$$

where R is the total discounted revenue, V is the value of electricity (assumed to be 100 dollars per megawatt-hour in this study), δ is the discount factor (assumed to be 10% in this study), and t is measured in years. We focus on a "lifetime" revenue quantity, where the wind farm lifetime is approximated with a small time period of $T = 10$ years. This choice is conservative for the presented sensitivity analysis, as longer horizons would increase exposure to neighboring farm effects.

Ten years of daily average wind speed and direction data, taken from the New European Wind Atlas [8], is used to characterize the wind energy resource. As simplifications, we assume a uniform wind resource, taken at the center of the target wind farm (e.g., that there is no spatial variability in the inflow speed and direction). We assume a shear coefficient of 0.05.

In this study, uncertainty in neighboring wind farms is quantified in terms of the anticipated construction time of each neighboring farm, the turbines used in each neighboring farm, and the layout of each neighboring farm. Each wind farm has a nameplate capacity of approximately 1 GW. The number of turbines per farm is determined by the floor of 1 GW divided by the rated power of the selected turbine type, yielding 66–100 turbines depending on turbine type. The target wind farm (the central one being designed) has 66 15 MW turbines.

The turbine type is represented as the rated power, which controls the rotor diameter,

$$\mathrm{RD} = 240\sqrt{\frac{\mathrm{RP}}{15}} \tag{2}$$

and hub height,

$$\mathrm{HH} = \mathrm{RD}\frac{150}{240}\,. \tag{3}$$

Neighboring wind farm turbine types are parameterized via the rated power, which is drawn uniformly from $\{10, 11, 12, 13, 14, 15\}$ MW. The turbine thrust curves are determined using 1-D momentum theory, which is not affected by these parameters. The rotor diameter and hub height are the key characteristics of the neighboring wind farms that influence the external wake effects.

Uncertainty in neighboring wind farms is approximated by using several solutions to the *smart-start* optimization algorithm, which is a greedy optimization algorithm that sequentially places turbines to maximize the AEP of the next-placed turbine [9]. Layout uncertainty is represented by adjusting the random number seed between 200 unique values, using 20% random percent in the TOPFARM implementation (controlling how many near-optimal grid positions are considered when placing each turbine) [9, 10].

The build time is nominally represented using a uniform distribution,

$$\text{construction day}(t) \sim \frac{t}{T} \tag{4}$$

where T is the anticipated total life time of the wind farm and $t \in [0, T]$.

After the surrogate is selected, it is challenged to predict the distribution of cumulative discounted revenues associated with different uncertainty scenarios. In particular, we change the construction time uncertainty from a uniform distribution to an exponential distribution, with various time scales,

$$\text{construction day}(t) \sim \frac{1}{\lambda}\exp(-\frac{t}{\lambda}) \tag{5}$$

where λ is a time scale that can be set arbitrarily.

The wind farm construction day, turbine type, and turbine arrangement parameters represent three important types of random variables. The wind farm construction days are drawn from continuous distributions. The turbine types are drawn from integer distributions. The turbine locations are selected from several draws of complicated joint probability distributions that can only be parameterized with a random number seed. The latter is a sort of black box approach; a set of parameters could be derived to deterministically control where each turbine is placed in the smart-start algorithm, but this would involve significant code changes and introduce an exponentially larger input space.

2.1. Surrogate-Based Sensitivity Analysis

To better understand this problem, we construct a surrogate to assist in understanding the sensitivity of the revenue to different inputs. We examine four candidate surrogate modeling

approaches. These candidates are artificial neural network, random forest, linear regression, and polynomial regression with sliced inverse regression (SIR) dimension reduction.

The Tensorflow library is used to construct feed forward neural networks with different parameterizations [11]. Similarly, the Extreme Gradient Boosting (XGBoost) package is used to construct random forest models given a set of hyperparameters [12]. Linear regression is performed using the Scikit-Learn package [13]. The sliced python package is used to perform sliced inverse regression, and the reduced dimension is used to construct one-dimensional polynomial surrogates with Scikit-Learn.

There is ambiguity in the appropriate distribution of construction day. This is because there is very little information available to developers regarding the characteristics of neighboring wind farms. It would be ideal to construct a surrogate that performs wells out of distribution, so that an intelligence team can easily update the assumed distributions based on the latest available information.

Each surrogate is selected via a k-fold hyper-parameter sweep. During this selection, described in appendix A, the uniformly sampled data is split into different training and testing sets, and the average absolute bias is reported for each hyperparameter combination using 5 folds.

Sensitivity is typically quantified using Sobol indices or the closely related SHapley Additive exPlanations (SHAP) index. We use the sampling method proposed by Saltelli [14] to sample the selected surrogate model and compute first- and total-order Sobol indices. These estimates are corroborated using SHAP indices estimated via the shap Python package [15].

The Sobol main effects index is defined as

$$M_j = \frac{1}{\mathrm{Var}\left[f\left(x\right)\right]} \mathrm{Var}_{\boldsymbol{x}_j}\left[\mathbb{E}_{\boldsymbol{x}_{\sim j}}\left(f\left[\boldsymbol{x}\right]\right)\right] . \tag{6}$$

By sampling the power and layout according to a fixed set of values, the main effects index can be directly computed. The sampled data can be sorted by unique values of x_i, allowing for the computation of the expected value of $f(x)$ for each j, then taking the variance across j.

We rely on a hybrid approach for sensitivity analysis. For continuous variables (construction time, rated power), we utilize the gradient-boosted tree surrogate (XGBoost) to compute Sobol indices efficiently. However, the neighbor layout is a discrete, unordered variable (random seed), which renders standard regression-based sensitivity metrics ineffective. For this variable, we employ a direct variance-based Sobol computation using a "Pick-Freeze" method to directly estimate main Sobol effects indices based on the raw simulation data using Equation 6. We refer to this as "direct estimation" throughout the remaining text, to distinguish it from surrogate-based Sobol computation.

The sliced inverse regression (SIR) algorithm organizes the data by slicing the output into chunks, then performing an eigendecomposition of the average value of the inputs within each chunk [16]. This is suitable for assessing the construction day and rated power uncertainties, as we can expect a somewhat smooth response surface, but not for the layout uncertainty seeds, where the average is meaningless. The eigenvectors yielded by the SIR analysis is an indication of parameter sensitivity. We compute the eigenvalue-weighted sum of the squared components of the first three eigenvectors, normalized to sum to one, to capture the input's contribution across the primary dimensions of variation in the output.

While Sobol indices, SHAP values, and SIR-based metrics have distinct theoretical foundations, all three quantify how much each input contributes to output variation; their agreement here provides cross-validation of the sensitivity rankings.

The sensitivity analysis described above identifies which uncertain inputs most strongly influence revenue variance. However, there is significant ambiguity in the appropriate probability distributions to assign to these inputs. Developers may have limited intelligence on competitors' timelines/designs, and available information will likely evolve over time. To address this, we use the surrogate model to rapidly evaluate revenue risk metrics under a range of distributional assumptions. Specifically, we examine the 90th percentile probability of exceedance (P90) revenue under exponential construction time distributions (truncated at the project lifetime T) with varying time scales (λ in Equation 5). Note that the surrogate training data uses standard (non-truncated) exponential distributions, where sampled construction times exceeding the project lifetime result in zero interaction—effectively representing canceled or indefinitely delayed projects. This distinction means the P90 analysis constitutes a mild out-of-distribution evaluation, further validating the surrogate's robustness.

This analysis quantifies how sensitive financial risk is to the assumed arrival distribution, beyond what variance-based sensitivity indices capture. Because this application requires evaluating the surrogate on distributions different from its training data, out-of-distribution (OOD) generalization is critical. Appendix A details the surrogate selection process, which explicitly validates candidate models against exponential distributions after training on uniformly-distributed samples. The selected XGBoost model demonstrates robust OOD performance, enabling reliable scenario analysis across a range of plausible construction time assumptions.

2.2. Optimization Problem Statement

We examine the Danish energy island site, using 10 years of data from the New European Wind Energy Atlas [8]. The wind farm boundaries, location probability distributions, and the site wind rose are shown in Figure 1.

The time series associated with a uniform distribution of construction days are visualized in Figure 2. The average values across time and samples are reported in Table 2.

TABLE 2: Wake losses averaged over time and Monte Carlo samples.

Quantity	Wake Loss (%)
No Wakes	–
Internal Wakes Only	6.04
External Wakes Only	4.63
Total Wake Losses	9.88

We then optimize layouts using deterministic assumptions and stochastic formulations. In all cases, we use the stochastic

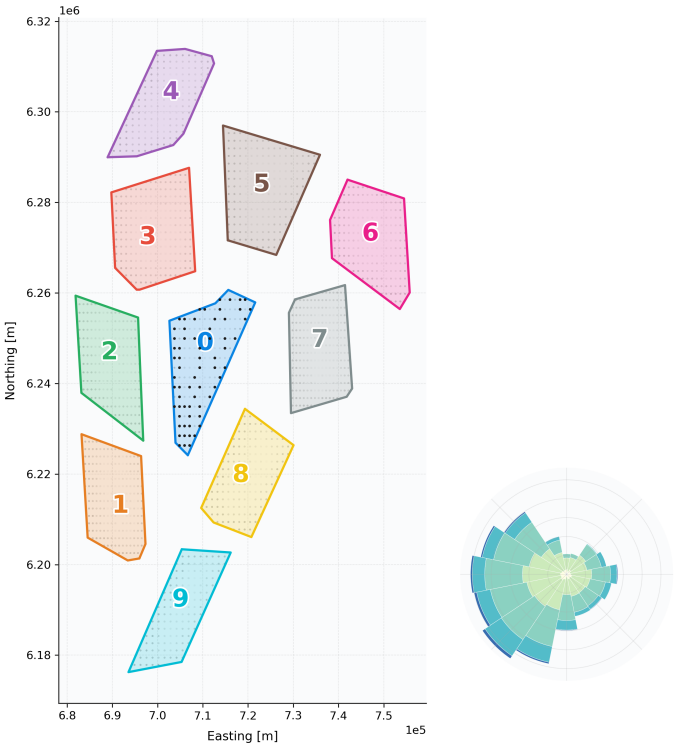

FIGURE 1: Wind farm boundaries and the distributions of turbine positions found by sampling smart start. Each wind farm is labeled. The site wind rose is visualized in the lower right corner.

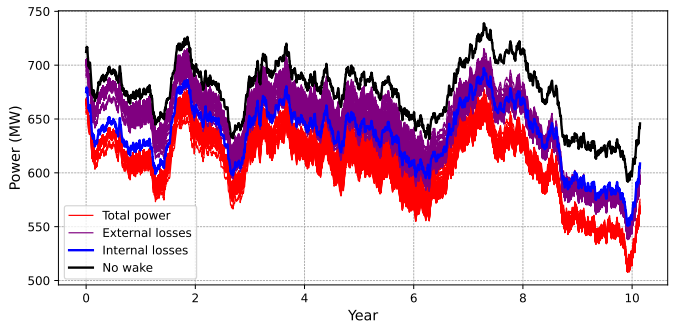

FIGURE 2: One-year rolling average of total power, power with external wakes, power with internal wakes, and power with internal and external wakes.

gradient descent driver in TOPFARM to perform the optimization. The general optimization statement is

$$\max_{\boldsymbol{x},\boldsymbol{y}} \mathbb{E}[AEP] \tag{7}$$

subject to

$$(x_i - x_j)^2 + (y_i - y_j)^2 \geq (N_D D)^2 \quad \forall i, j > i \tag{8}$$

$$d(x_i, y_i) > 0 \quad \forall i \tag{9}$$

where N_D is a free parameter controlling the minimum spacing between turbines in units of turbine rotor diameters (three in this case study), D is the turbine rotor diameter, and d is the distance outside of acceptable farm boundaries.

In our approach, AEP (more specifically, the gradient of AEP) is estimated via Monte Carlo simulation:

$$\mathbb{E}[AEP] \approx 8760 \frac{1}{N} \sum_{k=1}^{N} P(u^{(k)}, \theta^{(k)}, \boldsymbol{\mathcal{B}}^{(k)}, \boldsymbol{\mathcal{P}}^{(k)}, \boldsymbol{\mathcal{S}}^{(k)}) \tag{10}$$

where N is the mini-batch size, u is the freestream velocity at 150 m, θ is the freestream wind direction at hub height, $\boldsymbol{\mathcal{B}}$ is a vector describing the build times of each neighboring wind farm, $\boldsymbol{\mathcal{P}}$ is a vector of rated powers of the neighboring wind farms, and $\boldsymbol{\mathcal{S}}$ is the set of seeds corresponding to the assumed neighboring wind farm layouts.

While this framework supports a full optimization under uncertainty formulation, for the purpose of this study, we simplify the problem into two bounding scenarios to clearly quantify the design trade-offs:

1. **The "Liberal" Scenario:** We assume the target farm operates in isolation ($\boldsymbol{\mathcal{B}} \to \infty$). This represents an optimistic baseline where no external wakes are present.

2. **The "Conservative" Scenario:** We assume all 9 neighboring wind farms are fully built and operational at the start of the project ($\boldsymbol{\mathcal{B}} = 0$) with fixed layout seeds and 15 MW turbines.

For each random initial layout, we first maximize the expected AEP assuming the target farm operates in isolation. This phase performs a global exploration of the design space using the TOPFARM Stochastic Gradient Descent (SGD) driver [10, 17]. To encourage exploration and escape local minima, a high initial learning rate is employed. Then, using that solution as a starting point, we refine the layout to maximize AEP for the Conservative scenario. This "Liberal-to-Conservative Refinement" strategy allows us to measure the geometric stability of the layout: if the optimal layout changes significantly between scenarios, the design is sensitive to neighbor presence; if it remains static, the design is robust. The SGD hyperparameters employed for the initial liberal search and conservative refinement stages are listed in Table 3. Note that the constant learning rate iterations parameter has been added to the TOPFARM library since the publication of the initial SGD paper.

3. RESULTS

This section presents the results of the analysis of neighboring wind farm wake effects in the Danish energy island case study. The surrogate model selection is relegated to Appendix A. An xgboost model is developed to have low cross-validation errors within and outside its training distribution. This xgboost model is relied on in these results. Section 3.1 shows the sensitivity metrics yielded by the analysis of the sensitivity of lifetime revenue with respect to each of the uncertain inputs. It also analyzes the sensitivity of the revenue of a nominal layout with respect to assumed neighboring wind farm build times. Section 3.2 outlines the differences between the layouts associated with the conservative and liberal design approaches.

3.1. Sensitivity Analysis

In Figure 3, the sensitivity of the ten-year revenue with respect to each uncertain variable is shown, averaged across the different wind farms. Sensitivity is quantified using the direct estimation of Sobol indices discussed in the Methodology. We find that wind farm construction day is by far the most impactful uncertainty, and focus on this uncertainty source for the remainder of the analysis.

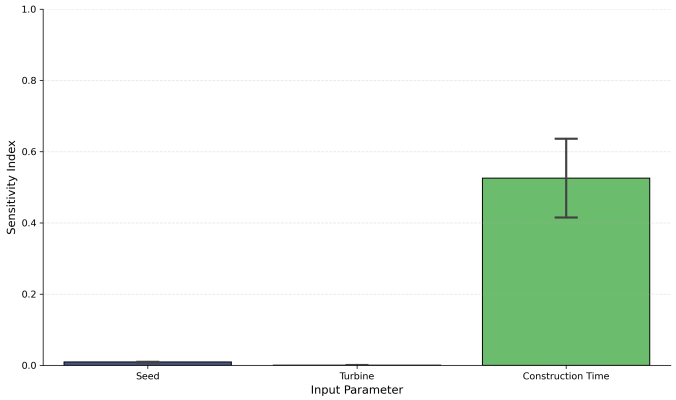

FIGURE 3: Direct estimation (pick-freeze method on raw simulation data) of the main Sobol effects index of lifetime revenue with respect to layout seed, turbine type, and construction time. Results are averaged across different farms and the error bars show the farm-to-farm standard deviation.

Figure 4 shows the sensitivity of the ten year revenue with respect to each wind farm's construction time. As the construction time is a continuous variable (as opposed to the categorical layout generation seed variable), several surrogate-based sensitivity analysis methods are available. The figure compares the results of the Saltelli Sobol estimates, computed SHAP values, and sensitivity metrics yielded via the SIR eigen-decomposition , which generally are all in agreement. The construction time of wind farm 2, which is the closest farm in the westerly/dominant wind direction, is the most impactful variable on the ten year revenue.

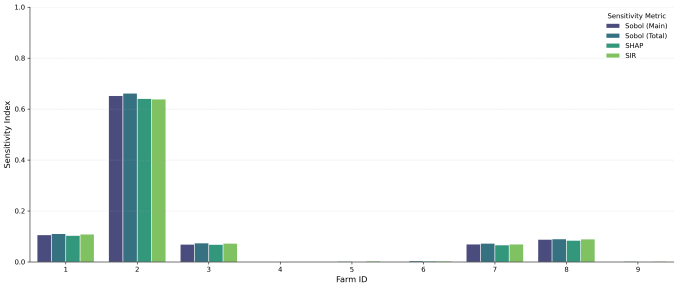

FIGURE 4: Sensitivity of lifetime revenue with respect to the construction time of each neighboring wind farm. The different sensitivity metrics considered are shown with different colors.

While the Sobol indices identify Construction Time as the dominant driver of variance, they do not quantify the directional risk associated with the uncertainty distribution itself. To understand this, we used the surrogate to estimate the 90th percentile (P90) probability of exceedance for the baseline revenue across a range of exponential time scales, λ.

Figure 5 illustrates this relationship. Low values of λ (corresponding to a rapid neighbor build-out) result in a sharp decrease in the P90 revenue, confirming that the financial downside is heavily concentrated in scenarios where neighbors arrive early. This non-linear sensitivity to the arrival distribution highlights the danger of relying on a single "most likely" construction schedule. The steep slope at low λ highlights the danger of overly pessimistic assumptions: assuming all neighbors will certainly be present results in revenue projections substantially below what may be realized if competitor build-out is even modestly delayed. This could lead developers to reject viable projects or undervalue assets. Conversely, the flattening at high λ shows diminishing returns to an "optimistic" uniform distribution. This asymmetry suggests that gathering intelligence to rule out the most pessimistic scenarios may be more valuable than confirming optimistic ones.

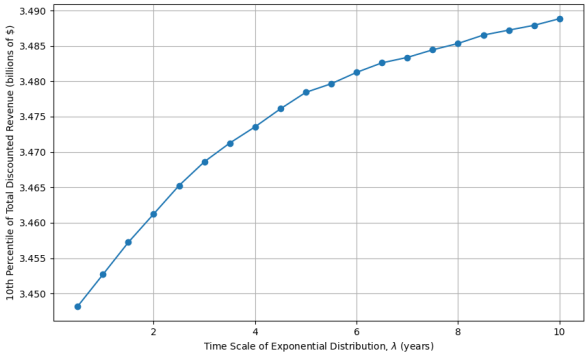

FIGURE 5: Sensitivity of the P90 revenue metric to the assumed construction time scale (λ). The steep slope at low λ indicates significant financial risk associated with early neighbor arrival.

Consequently, rather than optimizing for a single uncertain distribution (which might be incorrect), the subsequent layout optimization focuses on the bounding scenarios identified here: the "Liberal" case (neighbors never arrive, $\lambda \to \infty$) and the "Conservative" case (neighbors arrive immediately, $\lambda \to 0$).

3.2. Conservative Versus Liberal Design

We perform optimization using liberal (no neighbors) and conservative (neighbors are present) scenarios, using ten initial random layouts. As discussed in the Methodology, conservative optimization runs are carried out as refinements of liberal optimization solutions. The resulting Pareto set is shown in Figure 6. This analysis reveals no optimization trade-offs between the conservative and liberal scenarios—there is a single dominant point in the identified Pareto set. The liberal evaluations of each solution range between around 5460 and 5500 GWh (0.7% variation) and the conservative evaluations range between about 4680 and 4710 (0.6% variation). The identified dominant point is an outlier in the sense that the conservative refinement did not yield an improvement. Most conservative refinement runs yielded small

benefits (about 0.01% increase in conservative AEP). Based on these results, we conclude there are no trade-offs between liberal and conservative AEP for this particular wind farm cluster. If tradeoffs exist, they are almost certainly of a very small magnitude.

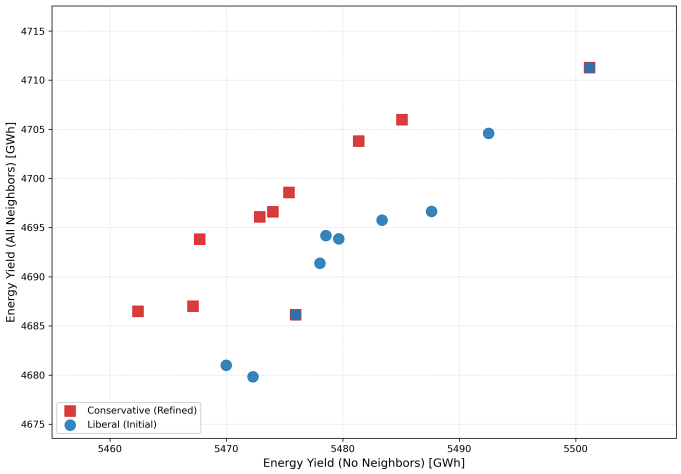

FIGURE 6: Pareto set discovered between conservative and liberal design scenarios. Layouts are originally optimized for the liberal case (blue circles). Then they are refined for the conservative case (red squares).

4. CONCLUSIONS

This study outlines a framework for rapid scenario testing when considering neighboring wind farm effects. It presents a detailed surrogate-based sensitivity analysis of neighboring wind farm effects and suggests a framework for dealing with ambiguity in these quantities.

The sensitivity analysis revealed that neighboring wind farm construction time is a much more important factor than neighboring wind farm turbine types or layout when considering lifetime revenue in the Danish Energy Island wind farm cluster case. It was found that there is a danger in being overly-pessimistic, in the sense that projecting the timeline of neighboring wind farm construction times slightly further into the future from a target wind farm's construction day can have a large effect on the revenue.

Based on the presented sensitivity analysis and optimization results, we conclude that it is not necessary to perform optimization under uncertainty in this setting. There would only be sense to this if there were tradeoffs revealed by making different assumptions that are impactful to the lifetime revenue. These findings are conditional on a single cluster geometry, one wake model parameterization, and a limited optimization sample. Design tradeoffs may emerge under different site configurations or modeling assumptions. Future work may include extending framework to include wake model and wind resource uncertainties, constructing time-varying surrogates for high-resolution sensitivity analysis, and examining when design tradeoffs may occur in wind farm cluster applications.

5. ACKNOWLEDGEMENTS

This work was partially funded by Shell and TotalEnergies. The authors gratefully acknowledge PJ Stanley, Jasper Kreeft, and Mikkel Friis-Møller for their valuable contributions and support.

AI Tools Disclosure: Claude 3.5 Opus (Anthropic, claude.ai, accessed via web browser, November 2025-January 2026) was used to review the manuscript for clarity. Gemini (Gemini 3 Pro, Google, gemini.google.com, accessed via web browser, November 2025-January 2026) was used to cross-reference the Python codebases with the manuscript and to accelerate the development of boilerplate code, parallelization routines, and data I/O handling for the computational framework (Python 3.14). All physical models, wake deficit parameterizations, sensitivity analysis methodologies, surrogate model selection, and optimization formulations were manually defined and verified by the authors to ensure scientific accuracy. The authors reviewed all AI suggestions and retain full responsibility for the content and integrity of this work.

REFERENCES

[1] Wiser, Ryan, Lantz, Eric, Mai, Trieu, Zayas, Jose, DeMeo, Edgar, Eugeni, Ed, Lin-Powers, Jessica and Tusing, Richard. "Wind vision: A new era for wind power in the United States." *The Electricity Journal* Vol. 28 No. 9 (2015): pp. 120–132.

[2] Platis, Andreas, Siedersleben, Simon K, Bange, Jens, Lampert, Astrid, Bärfuss, Konrad, Hankers, Rudolf, Cañadillas, Beatriz, Foreman, Richard, Schulz-Stellenfleth, Johannes, Djath, Bughsin et al. "First in situ evidence of wakes in the far field behind offshore wind farms." *Scientific reports* Vol. 8 No. 1 (2018): p. 2163.

[3] Fischereit, Jana, Schaldemose Hansen, Kurt, Larsén, Xiaoli Guo, van der Laan, Maarten Paul, Réthoré, Pierre-Elouan and Murcia Leon, Juan Pablo. "Comparing and validating intra-farm and farm-to-farm wakes across different mesoscale and high-resolution wake models." *Wind Energy Science* Vol. 7 No. 3 (2022): pp. 1069–1091.

[4] O'Neill, Niall, Réthoré, Pierre-Elouan, Mouradi, Rem-Sophia, Mathieu, Antoine and Quick, Julian. "Wind Farm Layout Optimization Accounting for Uncertainty in Model Selection." *Journal of Physics: Conference Series*, Vol. 3016. 1: p. 012054. 2025. IOP Publishing.

[5] Van Der Laan, MP, García-Santiago, O, Sørensen, NN, Troldborg, N, Risco, J Criado and Badger, J. "Simulating wake losses of the Danish Energy Island wind farm cluster." *Journal of Physics: Conference Series*, Vol. 2505. 1: p. 012015. 2023. IOP Publishing.

[6] GoBe Consultants, Anatec. "Outer Dowsing Offshore Wind Environmental Statement: Chapter 18 Marine Infrastructure and Other Users." (2024). Prepared for Development Consent Order Application.

[7] Nygaard, Nicolai Gayle, Poulsen, Lasse, Svensson, Erik and Pedersen, Jesper Grønnegaard. "Large-scale benchmarking of wake models for offshore wind farms." *Journal of Physics: Conference Series* Vol. 2265 (2022): p. 022008. DOI 10.1088/1742-6596/2265/2/022008.

[8] Hahmann, Andrea N, Sile, Tija, Witha, Björn, Davis, Neil N, Dörenkämper, Martin, Ezber, Yasemin, García-Bustamante, Elena, González Rouco, J Fidel, Navarro, Jorge, Olsen, Bjarke T et al. "The making of the new European Wind Atlas, Part 1: model sensitivity." *Geoscientific Model Development Discussions* Vol. 2020 (2020): pp. 1–33.

[9] Valotta Rodrigues, Rafael, Pedersen, Mads Mølgaard, Schøler, Jens Peter, Quick, Julian and Réthoré, Pierre-Elouan. "Speeding up large-wind-farm layout optimization using gradients, parallelization, and a heuristic algorithm for the initial layout." *Wind Energy Science* Vol. 9 No. 2 (2024): pp. 321–341.

[10] Pedersen, Mads M, Friis-Møller, Mikkel, Réthoré, Pierre-Elouan, Riva, Riccardo, Quick, Julian, Krasimirov Dimitrov, Nikolay, Rinker, Jenni and Dykes, Katherine. "DTUWindEnergy/TopFarm2: Release of v2. 3.7." *Zenodo* .

[11] Abadi, Martín, Barham, Paul, Chen, Jianmin, Chen, Zhifeng, Davis, Andy, Dean, Jeffrey, Devin, Matthieu, Ghemawat, Sanjay, Irving, Geoffrey, Isard, Michael et al. "{TensorFlow}: a system for {Large-Scale} machine learning." *12th USENIX symposium on operating systems design and implementation (OSDI 16)*: pp. 265–283. 2016.

[12] Chen, Tianqi. "XGBoost: A Scalable Tree Boosting System." *Cornell University* (2016).

[13] Pedregosa, Fabian, Varoquaux, Gaël, Gramfort, Alexandre, Michel, Vincent, Thirion, Bertrand, Grisel, Olivier, Blondel, Mathieu, Prettenhofer, Peter, Weiss, Ron, Dubourg, Vincent et al. "Scikit-learn: Machine learning in Python." *the Journal of machine Learning research* Vol. 12 (2011): pp. 2825–2830.

[14] Saltelli, Andrea. "Making best use of model evaluations to compute sensitivity indices." *Computer physics communications* Vol. 145 No. 2 (2002): pp. 280–297.

[15] Lundberg, Scott M and Lee, Su-In. "A Unified Approach to Interpreting Model Predictions." Curran Associates, Inc. (2017). URL http://papers.nips.cc/paper/7062-a-unified-approach-to-interpreting-model-predictions.pdf.

[16] Li, Ker-Chau. "Sliced inverse regression for dimension reduction." *Journal of the American Statistical Association* Vol. 86 No. 414 (1991): pp. 316–327.

[17] Quick, Julian, Rethore, Pierre-Elouan, Mølgaard Pedersen, Mads, Rodrigues, Rafael Valotta and Friis-Møller, Mikkel. "Stochastic gradient descent for wind farm optimization." *Wind Energy Science* Vol. 8 No. 8 (2023): pp. 1235–1250.

TABLE 3: Hyperparameter used in the SGD optimization driver during liberal and conservative optimizations.

Parameter	Liberal Optimization	Conservative Optimization
Initial Layout Guess	Random	Liberal solution
Initial Learning Rate	20 m	10 m
Constant initial iterations	5,000	0
Decay iterations	2,000	2,000
Mini-batch size	32	32

APPENDIX A. SURROGATE MODEL VALIDATION UNDER DISTRIBUTION SHIFTS

In this study, we contrive a situation where we build a surrogate using uniformly distributed construction times, then to validate this with different distributions. The validation strategy is illustrated in Figure 7. Each model is trained by sampling from a uniform distribution of construction times with 5,000 samples, then evaluated using 2,000 independently generated distributions assuming uniform or exponential distributions of construction times. The exponential distributions are tested using exponential time scales of 1 and 2 years. For exponential validation distributions, construction times exceeding T are permitted during sampling; these cases contribute zero external wake losses, representing scenarios where the neighboring farm is not constructed within the project lifetime.

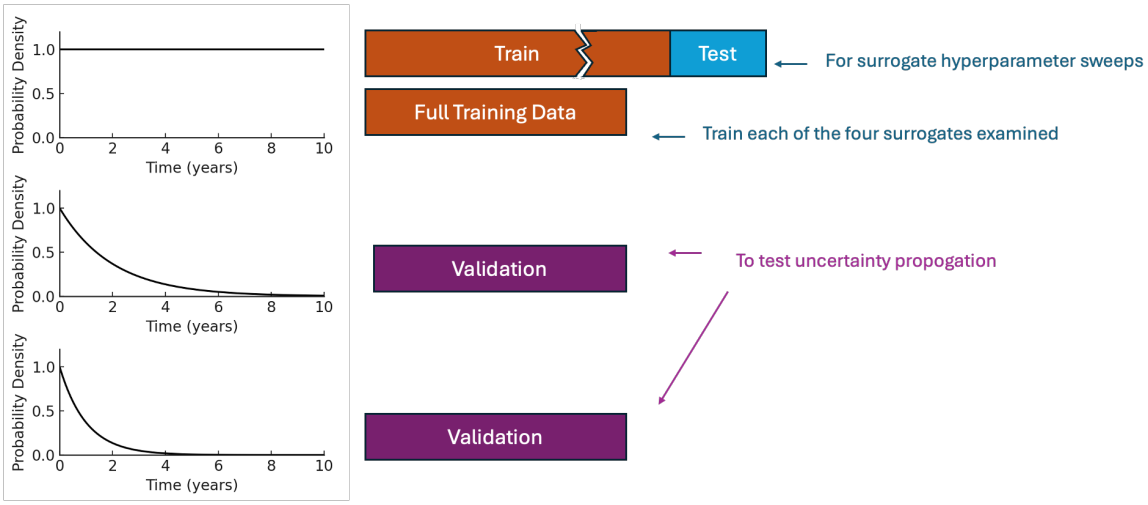

FIGURE 7: Datasets used in this analysis. The plots on the left show the assumed distributions of construction times. The uniform distribution is split into a train and test dataset for model selection. After a model is selected, it is trained using the full dataset associated with the uniform distribution. Then, the models are validated using exponential distributions of build time with different time scales.

The considered xgboost and neural network models were selected via a parameter search. The evaluated hyperparameters combinations are shown in Table 4. When considering neural network surrogates, we examine two distinct architectures. The "square" neural network architecture uses the same number of neurons in each layer. The "triangular" architecture linearly shrinks the number of layers until there is only one neuron in the final layer. The hyperparameter grid search is performed to minimize the root-mean-squared error in a validation set (e.g., independent draws of the uniform distribution used in the training data).

TABLE 4: Hyperparameter values examined in the parameter grid sweeps of the xgboost and neural network models.

Model	Parameter	Values
Neural Network	Number of Layers	2, 5, 10
	Neurons per Layer	5 10 25 50
	Activation Function	relu, tanh
	Batch Size	50, 100, 500
	Learning Rate	0.1, 0.01, 0.001
XGBoost	Learning Rate	0.1 0.01 0.001
	Maximum Depth	3, 6, 9
	Subsample Ratio	0.8, 0.9, 1.0
	Number of Estimators	100, 500, 1,000, 2,000, 5,000

In the OOD analysis, three metrics are used to quantify error under distribution shifts. They are

$$Bias = \frac{1}{N}\sum_{i=1}^{N}\left(R_i^{\text{obs}} - R_i^{\text{pred}}\right), \tag{11}$$

$$\text{RMSE} = \left[\frac{1}{N}\sum_{i=1}^{N}\left(R_i^{\text{obs}} - R_i^{\text{pred}}\right)^2\right]^{1/2}, \tag{12}$$

and

$$\text{KS} = \sup_R \left|F(R) - M(R)\right|, \tag{13}$$

where F and M are the cumulative distribution functions associated with the the probability density functions being compared.

Figure 8 shows the OOD predictions of the examined model when examining revenue in the first ten years. The XGBoost model outperforms the other models in OOD RMSE and KS. The triangular NN is the best for exp(2yr) bias, and is very close to xgboost in exp(1yr). The square NN model is remarkably inaccurate in the OOD cases, even though it has the lowest bias in the in-distribution validation data.

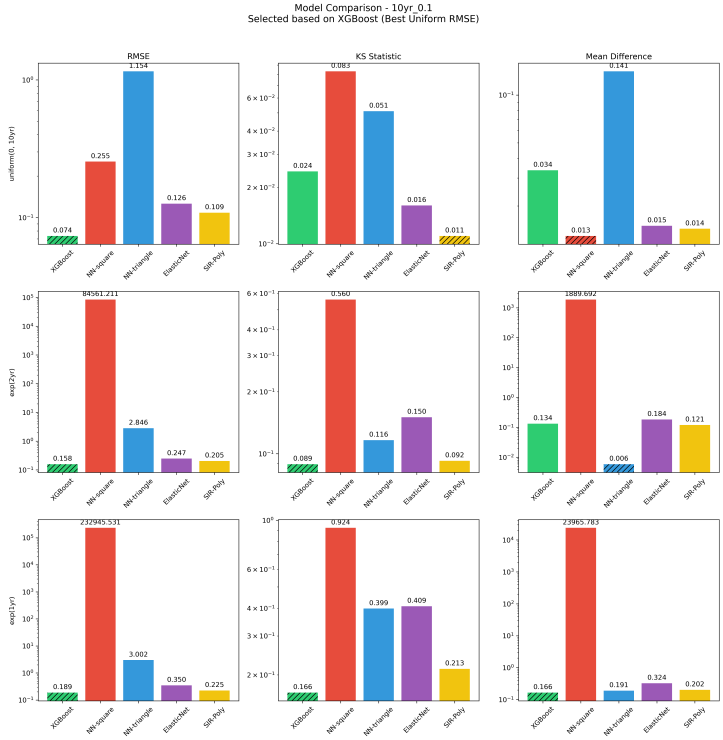

FIGURE 8: Comparison for OOD distributions for first 10 years of revenue